A&A 489, 589–600 (2008)
DOI: 10.1051/0004-6361:200809354

Astronomy & Astrophysics

Detection of vibrationally excited methyl formate in W51 e2

K. Demyk[1,⋆], G. Wlodarczak[1], and M. Carvajal[2]

[1] Laboratoire de Physique des Lasers, Atomes et Molécules, UMR CNRS 8523 Université Lille 1, 59655 Villeneuve d'Ascq Cedex, France
e-mail: Karine.demyk@cesr.fr
[2] Departamento de Fisica Aplicada, Facultad de Ciencias Experimentales, Universidad de Huelva, 21071 Huelva, Spain

Received 4 January 2008 / Accepted 30 June 2008

ABSTRACT

Context. Hot cores in molecular clouds, such as Orion KL, Sgr B2, W51 e1/e2, are characterized by the presence of molecules at sufficiently high temperatures to populate their low-frequency vibrationally excited states significantly. Complex organic molecules, such as methyl formate, ethyl cyanide or dimethyl ether, are characterized by a dense spectrum both in the ground state and in the excited states and lines from vibrationally excited states certainly participate to the spectral confusion.
Aims. Following a laboratory study of the first torsional excited mode of methyl formate, we search for methyl formate, $HCOOCH_3$, in its first torsionally excited state ($\upsilon_t = 1$) in the molecular cloud W51 e2.
Methods. We performed observations of the molecular cloud W51 e2 in different spectral regions at 1.3, 2, and 3 mm with the IRAM 30 m single dish antenna.
Results. Methyl formate in its first torsionally excited state ($\upsilon_t = 1$ at 131 cm^{-1}) is detected for the first time toward W51 e2. We detect 82 transitions among which 46 are unblended with other species. For a total of 16 A-E pairs in the observed spectrum, 9 are unblended; these 9 pairs are all detected. All transitions from excited methyl formate within the observed spectral range are detected and no strong lines are missing. The column density of the excited state is comparable to that of the ground state. For a source size of 7″, we find that $T_{\rm rot} = 104 \pm 14$ K and $N = 9.4^{+4.0}_{-2.8} \times 10^{16}$ cm^{-2} for the excited state and $T_{\rm rot} = 176 \pm 24$ K and $N = 1.7^{+.2}_{-.2} \times 10^{17}$ cm^{-2} for the ground state. Lines from ethyl cyanide in its two first excited states ($\upsilon_t = 1$, torsion mode at 212 cm^{-1}) and ($\upsilon_b = 1$, CCN in-plane bending mode at 206 cm^{-1}) are also present in the observed spectrum. Blending problems prevent a precise estimate of its abundance, although as for methyl formate, it should be comparable to the value derived for the ground state for which we find $T_{\rm rot} = 103 \pm 9$ K and $N = 3.7^{+0.6}_{-0.4} \times 10^{15}$ cm^{-2} for a 7″ source size.
Conclusions. With regard to the number of lines of excited methyl formate and ethyl cyanide detected in W51 e2, it appears that excited states of large molecules certainly account for a significant number of unidentified lines in spectral survey of molecular clouds.

Key words. ISM: molecules – ISM: abundances – ISM: individual objects: W51 e2 – radio lines: ISM – line: identification – methods: observational

1. Introduction

W51 e2 is a hot core part of the W51 H_{II} region located in the Sagittarius spiral arm at a distance of about 7–8 kpc. It is a region of high-mass star formation. W51 e2 and W51 e1 appear to be important star-forming cores. They exhibit a rich chemistry, comparable to that observed either in Orion or Sagittarius. Numerous large organic molecules have been observed in their direction. CH_3CN and CS maps were studied by Zhang et al. (1998). Formic acid (HCOOH) was mapped by Liu et al. (2001). Methyl formate ($HCOOCH_3$) and ethyl cyanide (CH_3CH_2CN) were observed in several studies (Liu et al. 2001; Ikeda et al. 2001; Remijan et al. 2002). Ikeda et al. (2001) studied ethylene oxide (c-C_2H_4O) and its isomer acetaldehyde (CH_3CHO). Acetic acid (CH_3COOH) was detected by Remijan et al. (2002) with a fractional abundance of $(1–6) \times 10^{-2}$ relative to $HCOOCH_3$. Glycine, whose presence may be inferred from the observations of acetic acid with which it shares common structural elements, was not detected in W51 e2 (Snyder et al. 2005). Trans-ethyl methyl ether was however detected in W51 e2 (Fuchs et al. 2005).

The rotational temperature of most of these large molecular species is high. Liu et al. (2001) estimated the rotational temperature in W51 e2 to be in the range 200–300 K. From high resolution observations of CH_3CN analyzed with statistical equilibrium models, Remijan et al. (2004) derived the kinetic temperature in W51 e2 to be $T_{\rm kin} = 153(21)$ K. At such temperature, low-energy vibrational excited states can be significantly populated. Transitions from vibrationally excited states have indeed been observed in other sources such as in Sgr B2(N-LMH) for C_2H_3CN, CH_3CH_2OH (Nummelin et al. 1998) and CH_3CH_2CN (Mehringer et al. 2004). Lines from torsionally excited methyl formate have been identified in Orion KL (Kobayashi et al. 2007).

In this study, we present the first detection of excited methyl formate and ethyl cyanide in the molecular cloud W51 e2. Our objective was to detect methyl carbamate (NH_2COOCH_3), an isomer of glycine (NH_2CH_2COOH), which has a larger dipole moment, making its detection more favorable than glycine. It was not detected. However, a few strong unidentified lines in the data attracted our attention and were attributed to methyl formate in its first torsional excited state. Further observations confirmed this assertion and lead to the detection of excited ethyl cyanide in W51 e2. The first vibrationally excited state of methyl formate

⋆ *Present address*: Centre d'Étude Spatiale des Rayonnements, Université Paul Sabatier, 31028 Toulouse, France.

is the CH_3 torsion mode, ν_{18}, hereafter referred to as $\upsilon_t = 1$, at 131 cm^{-1} (188 K). The rotational spectrum in this excited state was measured and analyzed by Ogata et al. (2004). Ethyl cyanide has two close vibrationally excited states, the CCN in-plane bending mode, ν_{13}, hereafter called $\upsilon_b = 1$, at 206 cm^{-1} (296 K) and the CH_3 torsion mode, ν_{21}, hereafter called $\upsilon_t = 1$, at 212 cm^{-1} (305 K). A preliminary analysis of the rotational spectrum in these two excited states is presented by Mehringer et al. (2004).

The observations and methods used for the data analysis are described in Sects. 2 and 3, respectively. The study of methyl formate and ethyl cyanide in the ground and excited state is presented in Sects. 4 and 5, respectively. The search for methyl carbamate and glycine is presented in Sect. 6. Our discussion is completed in Sect. 7.

2. Observations

The observations were performed with the IRAM 30 m antenna at Pico Veleta (Spain) in June 2003 and June 2006. W51 e2 was observed at the position $\alpha(2000) = 19°23'43.9''$ and $\delta(2000) = 14°30'34.8''$ in position switching mode with the OFF position located at $\alpha = 300''$ and $\delta = 0''$.

Several spectral windows in the 80–250 GHz range were observed to include as many transitions as possible for the searched molecules (excited methyl formate and ethyl cyanide for the 2006 data and methyl carbamate and glycine for the 2003 data) and as few transitions as possible of other molecules with numerous strong lines (such as methyl formate and ethyl cyanide in the ground state and dimethyl ether).

All lines were observed with an array of 4 receivers (in single-side band mode) set at the appropriate frequencies. The spectrometers used were a low resolution 1 MHz filter bank and an autocorrelator with a spectral resolution in the 40–320 kHz range, split between different receivers. Focus and pointing were checked regularly by observing the nearby ultra compact HII region K 3-50A. The rejection of the image band (USB) was about 26 dB at 3 mm, 12 dB at 2 mm, 15 dB at 1.3 mm, and 10 dB at 1.1 mm. The system temperature was typically 100–200 K, 200–700 K, 200–700 K, and 400–1500 K at 3, 2, 1.3, and 1.1 mm, respectively. The total usable ON + OFF integration time varied from 30 to 50 min depending on the frequency range. The beam size was 22″, 17″, and 10.5″ at 3, 2, and 1.3 mm, respectively. The spectra are presented in main beam temperature unit, which is calculated from the antenna temperature: $T_{mb} = F_{eff}/B_{eff} \times T_A^*$. The data were reduced using the GILDAS package.

3. Analysis

For the data analysis, we assume that local thermodynamic equilibrium (LTE) is reached, i.e. we assume that the excitation, rotational, and vibrational temperatures are equal to the kinetic temperature in the emitting region and that the lines are thermalized, i.e. their level population is described by a Boltzmann distribution at that temperature. The validity of this assumption is discussed in Sect. 7.

The data were analyzed using the classical rotational diagram method to estimate the rotational temperature and the column density with their uncertainties for the different identified species. We adopted the formulation from Turner (1991), corrected for beam dilution effects:

$$\ln\left(\frac{3kW}{8\pi^3\nu S\mu^2 g_i g_k}\right) = \ln\left(\frac{N}{Q}\right) - \frac{E_u}{kT} - \ln(b) \quad (1)$$

where W is the integrated line intensity in K km s^{-1}, ν the line frequency, $S\mu^2$ the line strength in Debye^2, g_i the reduced nuclear spin statistical weight, g_k the K-level degeneracy, Q is the partition function, E_u the upper state energy, N is the total column density, and T is the excitation temperature. Assuming a Gaussian beam, the beam dilution factor b is given by:

$$b = \frac{\theta_s^2}{\theta_s^2 + \theta_{tel}^2} \quad (2)$$

where θ_s and θ_{tel} are the source and telescope beam size in arcsecond, respectively.

Beam dilution effects were taken into account both in the rotational diagram analysis and in the emission modeling (see below). The emission region in W51 e2 was observed to be smaller than 10″ for most organic molecules (Remijan et al. 2002; Liu et al. 2001). Consequently beam dilution effects were important at low frequency at which the IRAM 30 m antenna beam size is significantly larger (29″ at 86 GHz).

We compared the observed spectrum with simulated spectra calculated using a simple emission model at local thermodynamic equilibrium (LTE). The expression for the simulated main beam temperature for one molecule was thus:

$$T_{mb} = b \times (J - J_{bg}) \times (1 - e^{-\tau}) \quad (3)$$

where J is the source function:

$$J = \frac{h\nu}{k} \times \left(e^{h\nu/kT} - 1\right)^{-1} \quad (4)$$

and

$$J_{bg} = \frac{h\nu}{k} \times \left(e^{h\nu/k\times 2.7} - 1\right)^{-1} \quad (5)$$

τ is the optical depth, summed over all the transitions of the molecules:

$$\tau = \sum_i \frac{c^2}{8\pi\nu^2} N_{tot} \frac{g_u}{Q} A_{ul} \Phi(\nu) e^{-E_l/kT} \left(1 - e^{-E_{ul}/kT}\right) \quad (6)$$

and $\Phi(\nu)$ is the line profile:

$$\Phi(\nu) = \frac{1}{\sqrt{\pi}\Delta\nu_D} \times e^{-(\nu-\nu_i)^2/\Delta\nu_D^2} \quad (7)$$

A_{ul} is the Einstein coefficient, E_{ul} the energy of the transition, E_l the energy of the lower state, g_u is the upper state degeneracy, Q the partition function, $\Delta\nu_D$ is the Doppler width of the line, b is the beam dilution correction factor, and N_{tot} is the total column density.

In hot cores, the temperature is such that the low-energy vibrational and/or torsional excited modes are significantly populated. We therefore used the vibrational-rotational partition function, Q_{rv}, instead of the pure rotational partition function. Assuming non-interacting harmonic vibrational levels and rigid rotor levels, the ro-vibrational partition function was approximated by (see Gordy & Cook 1984):

$$Q_{rv} = \prod_i \left(1 - e^{-h\nu_i/kT}\right)^{-d_i} \times Q_{rot} \quad (8)$$

where ν_i is the frequency of the vibrational mode i, d_i its degeneracy, and Q_{rot} is the rotational partition function. Q_{rot} is approximated by:

$$Q_{rot} = \sigma \times \sqrt{\frac{\pi(kT)^3}{h^3 ABC}} \quad (9)$$

where σ is the symmetry number (see Gordy & Cook 1984). At LTE, the temperature used to calculate the rotational and vibrational partition function was the same: we therefore assumed implicitly that $T_{\rm vib} = T_{\rm rot}$, hypothesis that may not be valid (see Sect. 7). For methyl formate that has one internal rotor, rotational transitions are split into A and E components and σ is equal to 2. To calculate the partition function, we considered the first excited state of methyl formate at 131 cm^{-1}. For ethyl cyanide, we used the partition function given by Mehringer et al. (2004), which is calculated by summing the rotational states of the ground state and the first two excited states of ethyl cyanide at 206 and 212 cm^{-1}. For methyl carbamate, we used the partition function in the ground vibrational state given by Groner et al. (2007).

4. Torsionally excited methyl formate

The predictions for the methyl formate lines are based on the work on this species by Carvajal et al. (2007). In this work, all experimental data available on the ground and excited states (3496 and 774 microwave lines, respectively) in the 7–200 GHz frequency range, covering the J values up to 43 in the ground state and up to 18 in the first excited state $\upsilon_t = 1$, were collected from previously published studies (Ogata et al. 2004; Oesterling et al. 1999; Plummer et al. 1986, 1984; Demaison et al. 1984). Carvajal et al. (2007) also added 434 new lines of methyl formate in the ground state, measured in Lille in the 567–669 GHz spectral range and corresponding to transitions with J and K values of up to 62 and 22, respectively. This dataset was fitted with almost experimental accuracy (root-mean-square deviations of 94 kHz and 84 kHz for the 3496 (774) lines of the ground torsional state and of the excited state $\upsilon_t = 1$, respectively) using the so-called rho axis method (RAM) described in the literature (Hougen et al. 1994) and a model extended to include perturbation terms through to the eighth order. The spectroscopic parameters and the details of the fitting procedure are given by Carvajal et al. (2007) in which a table presenting all the fitted experimental frequencies, measurement uncertainties, calculated frequencies, observed-calculated values, line strengths, energy levels as well as identifications of the transitions, is available as Supplementary data.

For the detection of lines in the W51 e2 spectrum, we provided a line-list of predicted line-center frequencies and line intensities based on an internal rotation model (RAM or Rho Axis Method). This method and the code[1] developed was used for several molecules detected in the interstellar medium: acetaldehyde, CH_3COH, (Kleiner et al. 1996), acetamide CH_3CONH_2, (Hollis et al. 2006), and acetic acid CH_3COOH, (Ilyushin et al. 2008). The laboratory measurements and predicted line frequencies of transitions in the first excited torsional state $\upsilon_t = 1$ of methyl formate in the spectral range used for the present detection are presented in Table 1 with the line assignment, the observed-calculated value, the experimental accuracy, the calculated uncertainty, the line strength, and the energy of the lower level[2].

More than eighty transitions from torsionally excited methyl formate, 82 precisely, are detected in the source among which 46 are not blended. Taking into account possible blending, we find that all lines from torsionally excited methyl formate, predicted to be sufficiently intense to be detectable, are present in the observed spectra. Furthermore, no lines, such as unobserved strong methyl formate lines, contradicts the identification in the observed spectral range. The internal rotation of the methyl group of methyl formate splits the transitions into A and E components of the same intensity. Among the 16 observed A-E pairs, 9 are not blended (see Fig. 1). The intensity of the lines in a A-E pair, when no lines of the pair is blended, is consistent with the expected ones, strengthening the identification of excited methyl formate in this source. The detected lines (observed frequency, integrated intensity, and line intensity) are listed in Table 2 with the laboratory or calculated frequency, the quantum numbers of the transition, its line strength, and lower state energy. The first column of Table 2 indicates the line number used to label the lines in Fig. 1. The number in parenthesis indicates the A or E line associated with the transition when it is observed. However, about half of the lines are blended. Comments were added in Table 2 to indicate line blenders when they are identified.

The non-blended lines were used to estimate the rotational temperature and column density of excited $HCOOCH_3$ using the rotational diagram method (Fig. 2, Table 4). Remijan et al. (2002) mapped W51 e2 with BIMA in two transitions of $HCOOCH_3$ at 228.629 GHz and 90.146 GHz. The size of the emission region in these lines was of about 7″ and 12″, respectively. Adopting these values for torsionally excited $HCOOCH_3$, we estimated a rotational temperature and a column density of $T_{\rm rot} = 131 \pm 20$ K and $N = 3.4^{+1.5}_{-1.1} \times 10^{16}$ cm^{-2}, respectively, for a source size of 12″, and $T_{\rm rot} = 104 \pm 14$ K and $N = 9.4^{+4.0}_{-2.8} \times 10^{16}$ cm^{-2}, for a source size of 7″ (Table 4). A separate analysis of the A and E lines of excited methyl formate provided compatible values, within the uncertainty, for the rotational temperature and column density. Transitions from the ground state of $HCOOCH_3$ were also detected. Using the rotational diagram method, we measured for $HCOOCH_3$ $\upsilon_t = 0$, $T_{\rm rot} = 199 \pm 28$ K and $N = 9.6^{+0.9}_{-0.9} \times 10^{16}$ cm^{-2} for a 12″ source (Fig. 3). If we consider both lines from the ground state and from $\upsilon_t = 1$, we find $T_{\rm rot} = 154 \pm 8$ K and $N = 5.6^{+4.0}_{-3.7} \times 10^{16}$ cm^{-2} for a 12″ source (Fig. 3, Table 4). These temperatures and column densities were used to model the emission of methyl formate in the source. The comparison of the modeled spectra with observations is shown in Fig. 1 for a number of lines from $HCOOCH_3$, $\upsilon_t = 1$.

5. Ethyl cyanide

Severals tens of lines from ethyl cyanide in the ground state are observed in the spectra. A large number of these lines are not blended and their energies cover a wide range, allowing us to plot a rotational diagram (Fig. 4). Adopting a source size of 12″ as for the ground state of methyl formate, we found a rotational temperature of $T_{\rm rot} = 114 \pm 11$ K and a column density $N = 1.7^{+0.3}_{-0.2} \times 10^{15}$ cm^{-2}. Adopting a smaller source of 7″ did not change the rotational temperature significantly but did alter the column density, such that $T_{\rm rot} = 103 \pm 9$ K and a column density $N = 3.7^{+0.6}_{-0.5} \times 10^{15}$ cm^{-2} (Table 4).

Ethyl cyanide appears to be colder than previously found. Liu et al. (2001) adopted a temperature of 200 K and measured an abundance for this molecule of 4×10^{15} cm^{-2}. However their analysis was based on lines of energies lower than 113 K. If we limit ourselves to low energy transitions, we find $T_{\rm rot} = 184$ K and a column density $N = 1.3 \times 10^{16}$ cm^{-2}. Ikeda et al. (2001)

[1] A version of the program is available at the web site (http://www.ifpan.edu.pl/~kisiel/introt/introt.htm#belgi) and other versions are available from Kleiner (see the web site for more information).

[2] A prediction of the overall spectrum of methyl formate in the ground and first excited states, for a large frequency range, will be published soon (Kleiner et al. in preparation).

Table 1. Laboratory measurements, calculated frequencies and line strengths for methyformate transitions in the first torsionally excited state used in the present detection.

J'	K'_a	K'_c	P'	J''	K''_a	K''_c	P''	Obs. Freq.	Calc. Freq.	Calc. Unc	Obs.-Calc.	$S\mu^2$	E_l
Upper state[a]				Lower state[a]				(MHz)[b]	(MHz)[c]	(kHz)[c]	(MHz)[c]	(D^2)	(cm^{-1})[d]
7	4	4	–	6	4	3	–	85 327.104	85 327.085	11	0.019	12.483	146.8606
7	4	3	+	6	4	2	+	85 360.669	85 360.823	11	–0.154	12.483	146.8610
7	3	5	+	6	3	4	+	85 371.762	85 371.789	11	–0.027	15.120	143.6253
7	–6	2		6	–6	1			85 456.630	19		4.944	155.5393
7	4	3		6	4	2		85 506.175	85 506.179	16	–0.004	12.571	146.6097
7	–5	3		6	–5	2		85 553.365	85 553.288	17	0.077	9.123	150.4139
10	2	9	–	10	1	10	+	85 664.038	85 663.943	20	0.095	1.403	151.8343
11	4	7	+	11	3	8	–	85 727.753	85 727.728	18	0.025	3.078	162.4132
7	–4	4		6	–4	3		85 743.967	85 743.894	16	0.073	12.532	146.2356
7	2	5	+	6	2	4	+	88 998.368	88 998.415	12	–0.047	17.049	141.4958
7	2	5		6	2	4		89 140.383	89 140.366	18	0.017	17.051	141.0232
25	5	20	–	25	4	21	+		107 021.644	361		8.289	274.8357
9	–2	8		8	–2	7		107 022.162	107 022.092	13	0.070	22.628	146.6924
10	1	9	–	9	2	8	–	107 472.351	107 472.387	15	–0.036	2.144	150.7587
9	–3	7		8	–3	6		111 005.617	111 005.582	19	0.035	20.800	149.1777
9	1	8		8	1	7		111 094.105	111 094.056	13	0.049	23.222	146.0900
12	0	12	+	11	0	11	+	131 536.624	131 536.653	12	–0.029	31.375	155.8502
12	0	12		11	0	11		131 612.344	131 612.301	13	0.043	31.558	155.3072
12	1	12	+	11	0	11	+	131 764.316	131 764.341	12	–0.025	4.870	155.8502
11	5	7	+	10	5	6	+	134 531.846	134 531.833	13	0.013	23.125	164.8530
27	7	20	–	27	6	21	+		134 545.609	582		8.581	304.5077
11	–7	5		10	–7	4		134 545.615	134 545.516	27	0.099	17.431	175.4588
35	8	27	+	35	7	28	–		134 553.290	912		12.622	416.6235
11	5	6	–	10	5	5	–	134 585.070	134 585.141	13	–0.071	23.125	164.8541
11	–3	9		10	–3	8		134 713.629	134 713.526	16	0.103	26.708	156.9827
11	5	6		10	5	5		134 739.630	134 739.629	19	0.001	23.251	164.7142
12	2	11	–	11	2	10	–	140 020.525	140 020.564	12	–0.039	30.616	158.9957
11	2	9	+	10	2	8	+	140 166.667	140 166.713	12	–0.046	28.103	155.9781
12	–2	11		11	–2	10		140 324.728	140 324.699	12	0.029	30.787	158.5211
13	–1	13		12	–1	12		142 032.334	142 032.293	14	0.041	34.222	159.7047
13	0	13	+	12	0	12	+	142 052.800	142 052.735	14	0.065	34.029	160.2378
13	0	13		12	0	12		142 125.416	142 125.410	14	0.006	34.224	159.6973
13	1	13	+	12	0	12	+	142 185.220	142 185.198	14	0.022	5.339	160.2378
15	0	15	+	14	1	14	+	163 042.398	163 042.248	20	0.100	6.267	170.0683
15	1	15	+	14	1	14	+	163 086.032	163 085.873	20	0.159	39.344	170.0683
15	0	15		14	–1	14		163 113.094	163 113.156	18	–0.062	6.073	169.5325
15	0	15	+	14	0	14	+	163 118.722	163 118.574	20	0.148	39.345	170.0657
14	1	13		13	1	12		163 142.587	163 142.607	14	–0.020	36.185	168.1362
15	–1	15		14	–1	14		163 154.325	163 154.404	18	–0.079	39.561	169.5325
15	0	15		14	0	14		163 185.864	163 185.922	18	–0.058	39.561	169.5300
15	–1	15		14	0	14		163 227.097	163 227.169	18	–0.072	6.074	169.5300
16	0	16	+	15	1	15	+	173 616.616	173 616.407	25	0.209	6.727	175.5082
16	1	16	+	15	1	15	+	173 641.411	173 641.171	25	0.240	42.007	175.5082
16	0	16	+	15	0	15	+	173 660.281	173 660.032	25	0.249	42.007	175.5068
16	0	16		15	–1	15		173 683.479	173 683.597	23	–0.118	6.525	174.9747
24	3	21	–	24	2	22	+		173 704.470	241		4.324	254.0651
16	–1	16		15	–1	15		173 706.683	173 706.807	23	–0.124	42.232	174.9747
16	0	16		15	0	15		173 724.731	173 724.845	23	–0.114	42.232	174.9733
16	–1	16		15	0	15		173 747.990	173 748.055	23	–0.065	6.525	174.9733
16	5	11		15	5	10		198 384.885	198 384.966	32	–0.081	38.205	191.3885
26	8	19	–	26	7	20	+		198 429.332	290		6.921	297.4256
16	5	11	–	15	5	10	–		198 539.350	30		38.279	191.5148
16	–5	12		15	–5	11		198 578.563	198 578.589	33	–0.026	38.090	191.0593
19	3	16	–	18	4	15	–		207 295.959	118		2.804	208.1331
17	12	5	+	16	12	4	+		207 354.058	101		12.640	252.9573
17	12	6	–	16	12	5	–		207 354.058	101		12.640	252.9573
17	–13	5		16	–13	4			207 376.777	145		18.783	264.5661
17	9	8		16	9	7			207 397.312	68		32.511	223.9160

Table 1. continued.

J'	K'_a	K'_c	P'	J''	K''_a	K''_c	P''	Obs. Freq. (MHz)[b]	Calc. Freq. (MHz)[c]	Calc. Unc (kHz)[c]	Obs.-Calc. (MHz)[c]	$S\mu^2$ (D^2)	E_l (cm^{-1})[d]
Upper state[a]				Lower state[a]									
17	11	7	+	16	11	6	+		207 404.993	81		26.248	242.2767
17	11	6	–	16	11	5	–		207 404.993	81		26.248	242.2767
17	10	8	–	16	10	7	–		207 500.297	66		29.526	232.5324
17	10	7	+	16	10	6	+		207 500.297	66		29.526	232.5324
19	2	18	–	18	1	17	–		215 130.469	47		6.562	199.2115
18	5	13	–	17	5	12	–		225 648.010	57		44.072	205.2072
19	2	17	+	18	2	16	+		225 702.569	46		48.659	203.7419
6	6	1	–	5	5	0	–		225 727.540	30		2.592	148.5921
6	6	0	+	5	5	1	+		225 727.552	30		2.592	148.5921
18	5	13		17	5	12			225 756.154	54		43.428	205.0713
7	6	1	+	6	5	2	+		237 899.077	27		2.594	151.0254
20	3	18	+	19	2	17	+		237 969.273	58		5.371	211.2706
37	7	31	+	37	6	32	–		238 027.934	1642		8.537	434.5487
20	–14	7		19	–14	6			244 000.464	195		27.134	299.1664
20	15	5	–	19	15	4	–		244 048.806	207		23.017	312.5791
20	15	6	+	19	15	5	+		244 048.806	207		23.017	312.5791
19	4	15	+	18	4	14	+		244 066.113	79		48.355	209.5678
27	1	26	–	27	0	27	+		244 066.575	470		1.456	268.2307
20	14	6	+	19	14	5	+		244 073.956	178		20.522	299.0954
20	14	7	–	19	14	6	–		244 073.956	178		20.522	299.0954
20	10	10		19	10	9			244 112.669	108		39.852	254.7516
20	13	7	–	19	13	6	–		244 119.960	154		24.670	286.5471
20	13	8	+	19	13	7	+		244 119.960	154		24.670	286.5471
20	12	8	+	19	12	7	+		244 198.512	134		34.020	274.9352
20	12	9	–	19	12	8	–		244 198.512	134		34.020	274.9352
20	–13	8		19	–13	7			244 207.619	159		30.739	286.5459

[a] Upper and lower state transitions quantum numbers. The rotational quantum number J, and the asymmetric rotor labels K_a and K_c are identified for each energy level. For the A symmetry species, P is the parity quantum number, for the E species, P is not defined, instead, the K_a label has a signed value (Hougen et al. 1994; Ilyushin et al. 2008). Note that this information has been suppressed in Table 2, otherwise the quantum number labeling is the same. [b] Observed laboratory frequencies in MHz from Ogata et al. (2004), the experimental uncertainty is 50 kHz for all measured lines; [c] calculated frequencies, uncertainties and obs-calc values are from (Carvajal et al. 2007) for the measured lines, the predicted frequencies and uncertainties for unmeasured lines is from Kleiner et al. (private communication); [d] lower state energy in cm^{-1}, relative to the $J = K = 0$ A species levels, set as zero energy.

Table 2. Detected transitions of the first torsionally excited state of $HCOOCH_3$ in W51 e2.

	Transition[a]	$S\mu^2$ (D^2)	E_l (cm^{-1})	Frequency (MHz)	Obs. Freq. [b] (MHz)	$\int T_{mb}\Delta v$[c] (K km s^{-1})	T_{mb} (mK)	Comment[d]
1(8)	7(4, 4)–6(4, 3) A	12.5	146.86	85 327.104	85 326.864	1.22	87	
2(5)	7(4, 3)–6(4, 2) A	12.5	146.86	85 360.669	85 359.685	0.40	81	
3	7(3, 5)–6(3, 4) A	15.1	143.62	85 371.762	85 371.871	0.67	102	
4	7(6, 2)–6(6, 1) E	4.94	155.53	85 456.630	85 456.067	14.33	1133	CH_3CCH
5(2)	7(4, 3)–6(4, 2) E	12.6	146.60	85 506.175	85 506.053	0.57	84	
6	7(5, 3)–6(5, 2) E	9.12	150.40	85 553.365	85 553.361	0.54	78	
7	10(2, 9)–10(1, 10) A	1.40	151.83	85 664.038	85 664.621	1.06	61	C_2H_3CN
8(1)	7(4, 4)–6(4, 3) E	12.5	146.22	85 743.967	85 743.915	0.79	102	
9(10)	7(2, 5)–6(2, 4) A	17.0	141.50	88 998.368	88 997.692	0.77	83	
10(9)	7(2, 5)–6(2, 4) E	17.1	141.01	89 140.383	89 140.161	1.20	120	
11	25(5, 20)–25(4, 21) A	8.29	274.84	107 021.644	107 021.862	1.99	186	
12	9(2, 8)–8(2, 7) E	22.6	146.68	107 022.162	–	–	–	
13	10(1, 9)–9(2, 8) A	2.14	150.76	107 472.351	107 472.400	0.27	45	
14	9(3, 7)–8(3, 6) E	20.8	149.16	111 005.617	111 005.832	2.67	261	
15	9(1, 8)–8(1, 7) E	23.2	146.08	111 094.105	111 094.010	2.27	244	
16(17)	12(0, 12)–11(0, 11) A	31.4	155.85	131 536.624	131 536.949	3.53	407	
17(16)	12(0, 12)–11(0, 11) E	31.6	155.29	131 612.344	131 612.094	3.97	410	
18	12(1, 12)–11(0, 11) A	4.87	155.85	131 764.316	131 765.100	1.70	100	$S^{18}O$
19	11(5, 7)–10(5, 6) A	23.1	164.85	134 531.846	134 531.411	3.44	478	SO_2 $\upsilon_2 = 1$
20	27(7, 20)–27(6, 21) A	8.58	304.51	134 545.609	134 546.431	7.95	630	$C_3H_2CN + {}^{33}SO_2$
21	11(7, 5)–10(7, 4) E	17.4	175.45	134 545.615	–	–	–	–
22	35(8, 27)–35(7,28) A	12.6	416.62	134 553.290	134 553.647	0.71	991	${}^{33}SO_2$
23(25)	11(5, 6)–10(5, 5) A	23.1	164.85	134 585.070	134 584.263	4.68	382	$C_3H_2CN\upsilon_t$, $\upsilon_b = 1$ and ?
24	11(3, 9)–10(3, 8) E	26.7	156.97	134 713.629	134 713.062	3.59	456	
25(23)	11(5, 6)–10(5, 5) E	23.3	164.70	134 739.630	134 739.110	3.55	386	

Table 2. continued.

	Transition[a]	$S\mu^2$ (D^2)	E_l (cm^{-1})	Frequency (MHz)	Obs. Freq.[b] (MHz)	$\int T_{mb}\Delta v$[c] (K km s^{-1})	T_{mb} (mK)	Comment[d]
26(28)	12(2, 11)–11(2, 10) A	30.6	159.00	140 020.525	140 020.145	2.96	472	
27	11(2, 9)–10(2, 8) A	28.1	155.98	140 166.667	140 166.502	3.42	528	
28(26)	12(2, 11)–11(2, 10) E	30.8	158.50	140 324.728	140 324.321	7.66	470	
29	13(1, 13)–12(1, 12) E	34.2	159.69	142 032.334	142 031.811	4.52	586	
30(31)	13(0, 13)–12(0, 12) A	34.0	160.24	142 052.800	142 052.867	5.95	724	
31(30)	13(0, 13)–12(0, 12) E	34.2	159.68	142 125.416	142 125.086	4.01	559	
32	13(1, 13)–12(0, 12) A	5.34	160.24	142 185.220	142 184.202	0.81	121	
33(35)	15(0, 15)–14(1, 14) A	6.27	170.07	163 042.398	163 042.050	2.32	363	
34(38)	15(1, 15)–14(1, 14) A	39.3	170.07	163 086.032	163 085.494	6.39	884	$HCOOCH_3$ $\upsilon_t = 0$
35(33)	15(0, 15)–14(1, 14) E	6.07	169.52	163 113.094	163 113.656	5.11	549	SO_2
36(39)	15(0, 15)–14(0, 14) A	39.3	169.52	163 118.722	163 118.285	19.40	2184	SO_2
37	14(1, 13)–13(1, 12) E	36.2	168.12	163 142.587	163 141.991	7.69	967	
38(34)	15(1, 15)–14(1, 14) E	39.6	162.52	163 154.325	163 153.604	8.99	855	
39(36)	15(0, 15)–14(0, 14) E	39.6	169.52	163 185.864	163 185.586	5.15	679	
40	15(1, 15)–14(0, 14) E	6.07	169.52	163 227.097	163 227.290	4.23	448	
41(44)	16(0, 16)–15(1, 15) A	6.73	175.51	173 616.616	173 617.000	1.80	177	
42(46)	16(1, 16)–15(1, 15) A	42.0	175.51	173 641.411	173 636.978	15.14	1288	$HCOOCH_3$ $\upsilon_t = 0$
43(47)	16(0, 16)–15(0, 15) A	42.0	175.51	173 660.281	173 659.384	4.12	380	
44(41)	16(0, 16)–15(1, 15) E	6.50	175.51	173 683.479	173 186.987	17.8	5300	CH_3CHO
45	24(3, 21)–24(2, 22) A	4.32	254.06	173 704.470	173 706.183	9.03	644	
46(42)	16(1, 16)–15(1, 15) E	42.2	174.96	173 706.683	173 706.183	–	–	
47(43)	16(0, 16)–15(0, 15) E	42.2	174.97	173 724.731	173 724.558	2.02	479	
48	16(1, 16)–15(0, 15) E	6.6	174.97	173 747.990	173 748.150	3.94	264	
49(51)	16(5, 11)–15(5, 10) E	38.2	191.37	198 384.885	198 384.516	5.23	467	
50	26(8,19)–26(7, 20) A	6.92	297.43	198 429.332	198 428.202	1.67	231	c-C_2H_4
51(49)	16(5, 11)–15(5, 10) A	38.3	191.52	198 539.350	198 541.500	19.44	1400	$HCOOCH_3$ $\upsilon_t = 0$
52	16(5, 12)–15(5, 11) E	38.1	191.05	198 578.563	198 577.928	3.20	484	
53	19(3, 16)–18(4, 15) A	2.8	208.13	207 295.959	207 296.361	5.16	159	CH_3CH_2CN
54	17(12, 5)–16(12, 4) A	21.2	252.96	207 354.058	207 352.197	5.57	557	
55	17(12, 6)–16(12, 5) A	21.2	252.96	–	–	–	–	
56	17(13, 5)–16(13, 4) E	18.8	264.55	207 376.777	207 378.506	11.46	995	CH_2NH
57	17(9, 8)–16(9, 7) E	32.5	223.90	207 397.312	207 396.134	8.62	758	
58	17(11, 6)–16(11, 5) A	26.2	242.28	207 404.993	207 404.612	5.67	690	
59	17(11, 7)–16(11, 6) A	26.2	242.28	–	–	–	–	
60	17(10, 8)–16(10, 7) A	29.5	232.53	207 500.297	207 499.521	4.8	897	
61	17(10, 7)–16(10, 6) A	29.5	232.53	–	–	–	–	
62	19(2, 18)–18(1, 17) A	6.56	199.21	215 130.469	215 130.828	2.59	394	CH_3CH_2CN
63(67)	18(5, 13)–17(5, 12) A	44.1	205.21	225 648.010	225 647.974	5.16	1103	$HCOOCH_3$ $\upsilon_t = 0$
64	19(2, 17)–18(2, 16) A	48.7	203.74	225 702.569	225 698.559	184	1400	H_2CO
65	6(6, 1)–5(5, 0) A	2.59	148.59	225 727.540	225 726.732	2.55	372	CH_2DCN
66	6(6, 0)–5(5, 1) A	2.59	148.59	225 727.552	–	–	–	–
67(63)	18(5, 13)–17(5, 12) E	43.4	205.06	225 756.154	225 755.178	7.3	927	
68	7(6, 1)–6(5, 2) A	25.6	229.84	237 899.08	237 896.263	15.91	1.667	NH_2CHO
69	20(3, 18)–19(2, 17) A	5.37	211.27	237 969.273	237 969.938	12.80	1.186	unidentified species
70	37(7, 31)–37(6, 32) A	8.54	434.55	238 027.934	238 026.742	1.12	122	
71	20(14, 7)–19(14, 6) E	27.1	299.15	244 000.464	243 999.803	7.82	596	
72	20(15, 6)–19(15, 5) A	23.3	312.58	244 048.806	244 048.230	90.33	10.84	H_2CS
73	20(15, 5)–19(15, 4) A	23.3	312.58	–	–	–	–	–
74	19(4, 15)–18(4, 14) A	18.4	209.57	244 066.113	244 066.720	5.49	730	
75	20(14, 7)–19(14, 6) A	14.2	299.10	244 073.956	244 073.440	3.54	314	unidentified species
76	20(14, 6)–19(14, 5) A	14.2	299.10	–	–	–	–	
77	20(10, 10)–19(10, 9) E	39.9	254.74	244 112.669	244 112.254	2.65	677	
78(82)	20(13, 8)–19(13, 7) A	21.0	286.55	244 119.960	244 119.708	2.95	886	
79	20(13, 7)–19(13, 6) A	21.0	286.55	–	–	–	–	
80	20(12, 8)–19(12, 7) A	34.0	274.94	244 198.512	244 198.232	7.43	1107	
81	20(12, 9)–19(12,8) A	34.0	274.94	–	–	–	–	
82(78)	20(13, 8)–19(13, 7) E	30.7	286.54	244 207.619	244 206.113	7.33	893	unidentified species

[a] The notation for the quantum numbers is the same as Table 1 except that it does not contain information on the parity of the level, i.e. the signs present in Table 1 (associated to K_a for the E species and in a separate column for the A species) have been suppressed; [b] observed frequencies for a systemic velocity of V_{lsr} = 55.3 km s^{-1}; [c] the line width is of the order of 7–8 km s^{-1}; [d] this column indicates the molecules blended with the detected $HCOOCH_3$ $\upsilon_t = 1$ transitions. The dashes indicates that the value is the same as the one in the previous line.

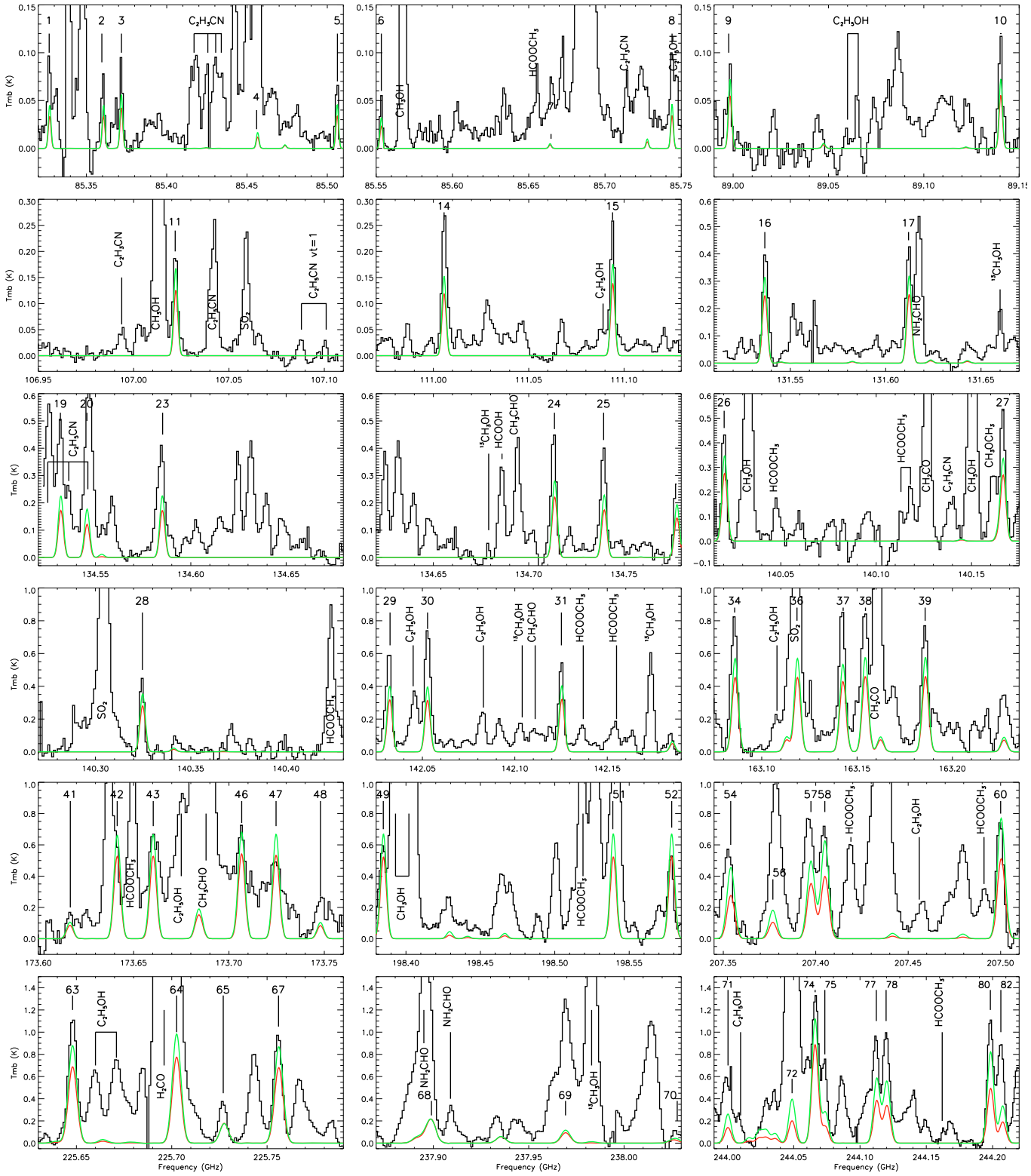

Fig. 1. Detected lines from the first torsionally excited state of methyl formate $HCOOCH_3$. The observations (histogram like curve) are compared with LTE emission models of $HCOOCH_3$ $\upsilon_t = 1$ with $\theta_s = 7''$, $T_{rot} = 104$ K and $N = 9.4 \times 10^{16}$ cm^{-2} (red curve) and with $\theta_s = 12''$, $T_{rot} = 154$ K and $N = 5.6 \times 10^{16}$ cm^{-2} (green curve). The numbered lines are transitions from torsionally excited $HCOOCH_3$, see Table 2 for the attribution of each line.

fixed T_{rot} to be 150 K and found a column density of $N = 7 \times 10^{14}$ cm^{-2}.

We searched for transitions from the first excited bending mode (in-plane CCN bending mode) of ethyl cyanide at 206 cm^{-1} (designated by $\upsilon_b = 1$), and from the first torsional excited state, $\upsilon_t = 1$, at 212 cm^{-1}. These 2 states and the CCN out-of-plane bending mode at 378 cm^{-1}, were studied by Fukuyama et al. (1999) in the 8–200 GHz range for $J \leq 16$ and $K_a \leq 2$. Lines from the two lowest energy states $\upsilon_b = 1$ and $\upsilon_t = 1$ were detected towards SgrB2 by Mehringer et al. (2004).

Table 3. Detected transitions of excited CH_3CH_2CN (υ_b = 1 and υ_t = 1) in W51 e2.

Transition	State	$S\mu^2$ (D^2)	E_l (cm^{-1})	Frequency (MHz)	Obs. Freq.[a] (MHz)	$\int T_{mb}\Delta v$[b] (K km s^{-1})	T_{mb} (mK)	Comment
$11_{8,4}-10_{8,3}$	υ_t = 1E	116.0	281.68	98 463.46	98 462.15	0.82	62	
$11_{8,3}-10_{8,2}$	υ_t = 1E	–	–	98 464.02	–	–	–	
$11_{8,4}-10_{8,2}$	υ_t = 1A	–	–	98 464.27	–	–	–	
$11_{8,3}-10_{8,3}$	υ_t = 1A	–	–	98 464.32	–	–	–	
$11_{9,3}-10_{9,2}$	υ_t = 1E	79.2	295.40	98 538.53	98 537.9	(c)	≤15	CH_3CH_2CN
$11_{9,2}-10_{9,1}$	υ_t = 1E	–	–	98 538.84	–	–	–	–
$11_{9,3}-10_{9,1}$	υ_t = 1A	–	–	98 539.10	–	–	–	–
$11_{9,2}-10_{9,2}$	υ_t = 1A	–	–	98 539.11	–	–	–	–
$11_{7,4}-10_{7,3}$	υ_b = 1E	156.3	258.45	98 556.61	98 557.5	(c)	≤50	(c)
$11_{7,5}-10_{7,4}$	υ_b = 1E	–	–	98 556.88	–	–	–	–
$11_{7,5}-10_{7,3}$	υ_b = 1A	–	–	98 557.12	–	–	–	–
$11_{7,4}-10_{7,4}$	υ_b = 1A	–	–	98 557.27	–	–	–	–
$11_{6,6}-10_{6,5}$	υ_b = 1E	188.1	248.92	98 617.87	98 619.1	2.2	105	(d)
$11_{6,5}-10_{6,4}$	υ_b = 1E	–	–	98 617.91	–	–	–	–
$11_{6,6}-10_{6,4}$	υ_b = 1A	–	–	98 618.09	–	–	–	–
$11_{6,5}-10_{6,5}$	υ_b = 1A	–	–	98 618.19	–	–	–	–
$11_{4,8}-10_{4,7}$	υ_t = 1A	237.0	242.51	98 619.45	–	–	–	–
$11_{5,7}-10_{5,5}$	υ_t = 1A	199.0	249.94	98 620.23	–	–	–	–
$11_{5,6}-10_{5,6}$	υ_t = 1A	–	–	98 620.33	–	–	–	–
$11_{4,8}-10_{4,7}$	υ_t = 1E	237.0	242.51	98 620.38	–	–	–	–
$11_{5,7}-10_{5,6}$	υ_t = 1E	212.8	249.94	98 620.41	–	–	–	–
$11_{4,7}-10_{4,6}$	υ_t = 1A	237.0	242.51	98 620.80	–	–	–	–
$11_{4,7}-10_{4,6}$	υ_t = 1E	–	–	98 620.82	–	–	–	–
$11_{5,6}-10_{5,5}$	υ_t = 1E	212.8	249.94	98 621.02	–	–	–	–
$11_{4,8}-10_{4,7}$	υ_b = 1A	240.4	234.40	98 735.64	98 736.0	0.38	31	
$11_{4,7}-10_{4,6}$	υ_b = 1E	233.2	–	98 735.77	–	–	–	
$11_{4,8}-10_{4,7}$	υ_b = 1E	–	234.40	98 738.68	98 738.8	0.57	75	
$11_{4,7}-10_{4,6}$	υ_b = 1A	240.4	–	98 739.06	–	–	–	
$12_{1,12}-11_{1,11}$	υ_b = 1E	297.2	229.03	107 088.63	107 088.5	0.52	50	C_2H_5OH ?
$12_{2,11}-11_{2,10}$	υ_b = 1A	–	229.03	107 088.81	–	–	–	–
$12_{2,11}-11_{2,10}$	υ_t = 1A	294.5	235.76	107 101.61	107 101.2	0.34	37	
$12_{1,11}-11_{1,10}$	υ_t = 1E	–	235.76	107 102.25	–	–	–	
$12_{8,4}-11_{8,3}$	υ_b = 1E	165.6	272.74	107 251.81	107 252.3	0.53	40	
$12_{8,5}-11_{8,4}$	υ_b = 1E	–	–	107 252.50	–	–	–	
$12_{8,5}-11_{8,3}$	υ_b = 1A	–	–	107 252.56	–	–	–	
$12_{8,4}-11_{8,4}$	υ_b = 1A	–	–	107 252.93	–	–	–	
$12_{8,5}-11_{8,4}$	υ_t = 1E	148.1	284.97	107 420.75	107 420.9	0.80	40	(d)
$12_{8,4}-11_{8,3}$	υ_t = 1E	–	–	107 421.34	–	–	–	–
$12_{8,5}-11_{8,3}$	υ_t = 1A	–	–	107 421.59	–	–	–	–
$12_{8,4}-11_{8,4}$	υ_t = 1A	–	–	107 421.66	–	–	–	–
$15_{4,12}-14_{4,11}$	υ_t = 1A	333.4	257.47	134 571.52	134 571.2	(c)	≤10	(c)
$15_{3,12}-14_{3,11}$	υ_t = 1E	329.8	257.47	134 576.01	–	–	–	–
$15_{3,13}-14_{3,12}$	υ_t = 1A	349.5	251.67	134 589.47	134 590.2	0.46	60	$HCOOCH_3\upsilon_t$ = 1
$15_{2,13}-14_{2,12}$	υ_t = 1E	–	–	134 590.45	–	–	–	–
$15_{6,10}-14_{6,9}$	υ_b = 1E	318.4	255.87	134 616.20	134 616.1	3.23	135	(d)
$15_{6,9}-14_{6,8}$	υ_b = 1E	–	–	134 616.38	–	–	–	–
$15_{5,11}-14_{5,10}$	υ_b = 1A	297.7	255.87	134 616.44	–	–	–	–
$15_{5,10}-14_{5,9}$	υ_b = 1A	–	–	134 616.58	–	–	–	–
$15_{11,5}-14_{11,4}$	υ_b = 1E	140.1	326.77	134 640.95	134 640.4	1.93	257	
$15_{11,5}-14_{11,3}$	υ_b = 1A	–	–	134 641.10	–	–	–	
$15_{11,4}-14_{11,3}$	υ_b = 1E	–	–	134 641.11	–	–	–	
$15_{11,4}-14_{11,4}$	υ_b = 1A	–	–	134 641.12	–	–	–	
$15_{12,4}-14_{12,3}$	υ_b = 1E	104.7	343.90	134 648.79	134 648.1	2.37	132	(d)
$15_{12,3}-14_{12,2}$	υ_b = 1E	–	–	134 648.90	–	–	–	–
$15_{12,4}-14_{12,2}$	υ_b = 1A	–	–	134 648.98	–	–	–	–
$15_{12,3}-14_{12,3}$	υ_b = 1A	–	–	134 649.00	–	–	–	–
$15_{10,6}-14_{10,5}$	υ_b = 1E	175.0	311.15	134 650.29	–	–	–	–
$15_{10,6}-14_{10,4}$	υ_b = 1A	–	–	134 650.34	–	–	–	–
$15_{10,5}-14_{10,5}$	υ_b = 1A	–	–	134 650.34	–	–	–	–
$15_{10,5}-14_{10,4}$	υ_b = 1E	–	–	134 650.49	–	–	–	–
$15_{13,3}-14_{13,2}$	υ_b = 1E	69.2	362.56	134 666.30	131 667.6	(c)	≤10	(c)
$15_{13,2}-14_{13,1}$	υ_b = 1E	–	–	134 666.33	–	–	–	–
$15_{13,3}-14_{13,1}$	υ_b = 1A	–	–	134 666.49	–	–	–	–
$15_{13,2}-14_{13,2}$	υ_b = 1A	–	–	134 666.50	–	–	–	–
$15_{9,7}-14_{9,5}$	υ_b = 1A	209.4	297.07	134 703.14	134 702.7	0.98	103	

Table 3. continued.

Transition	State	$S\mu^2$ (D^2)	E_l (cm^{-1})	Frequency (MHz)	Obs. Freq.[a] (MHz)	$\int T_{mb}\Delta v^b$ (K km s^{-1})	T_{mb} (mK)	Comment
$15_{9,6}-14_{9,6}$	υ_b = 1A	–	–	134 703.26	–	–	–	
$15_{9,7}-14_{9,6}$	υ_b = 1E	–	–	134 703.45	–	–	–	
$15_{9,6}-14_{9,5}$	υ_b = 1E	–	–	134 703.54	–	–	–	
$23_{0,23}-22_{0,22}$	υ_b = 1E	514.8	280.29	198 463.40	198 465.5	4.17	348	unidentified species
$23_{0,23}-22_{0,22}$	υ_b = 1A	–	–	198 463.42	–	–	–	–
$23_{4,19}-22_{4,18}$	υ_b = 1E	485.2	293.79	207 396.15	207 397.5	8.58	758	$HCOOCH_3\upsilon_t$ = 1
$23_{4,20}-22_{4,19}$	υ_b = 1A	–	293.79	207 396.27	–	–	–	–
$23_{1,22}-22_{1,21}$	υ_t = 1A	502.5	290.47	207 415.76	207 240.2	6.69	568	$HCOOCH_3\upsilon_t$ = 1
$23_{1,23}-22_{1,22}$	υ_t = 1E	–	290.47	207 417.59	–	–	–	–
$24_{0,24}-23_{1,23}$	υ_t = 1E	188.2	293.36	207 446.75	207 446.0	(c)	≤15	C_2H_5OH
$24_{0,24}-23_{1,23}$	υ_b = 1A	186.9	293.36	207 447.53	–	–	–	–
$24_{11,14}-23_{11,13}$	υ_t = 1E	325.5	393.52	215 133.09	215 132.5	(c)	≤380	unknown species
$24_{11,13}-23_{11,12}$	υ_t = 1E	–	–	215 133.41	–	–	–	–
$24_{11,14}-23_{11,12}$	υ_t = 1A	–	–	215 134.13	–	–	–	–
$24_{11,13}-23_{11,13}$	υ_t = 1A	–	–	215 134.19	–	–	–	–
$25_{4,21}-24_{4,20}$	υ_b = 1E	511.8	307.94	225 715.53	225 714.7	(c)	≤228	(c)
$25_{4,22}-24_{4,21}$	υ_b = 1A	–	–	225 715.61	–			
$27_{4,23}-26_{4,22}$	υ_b = 1E	534.4	323.30	244 142.10	244 139.3	3.94	288	
$27_{4,24}-26_{4,23}$	υ_b = 1A	–	–	244 142.13	–	–	-	
$28_{1,27}-27_{1,26}$	υ_t = 1A	539.3	327.94	250 318.38	250 316.2	2.7	298	
$28_{2,27}-27_{2,26}$	υ_t = 1E	269.5	327.94	250 319.81	–	–	–	
$28_{2,27}-27_{2,26}$	υ_t = 1E	–	–	250 319.81	–	–	–	
$28_{15,13}-27_{15,12}$	υ_b = 1E	273.8	486.17	251 372.86	251 373.7	(c)	≤10	(c)
$28_{15,14}-27_{15,13}$	υ_b = 1E	–	–	251 373.06	–	–	–	–
$28_{15,14}-27_{15,12}$	υ_b = 1A	–	–	251 373.29	–	–	–	–
$28_{15,13}-27_{15,13}$	υ_b = 1A	–	–	251 373.32	–	–	–	–

[a] Observed frequencies for a systemic velocity of V_{lsr} = 57 km s^{-1}; [b] the line width is of the order of 7–8 km s^{-1}; [c] line within the noise, a Gaussian fit could not be made, constrains the abundance of excited ethyl cyanide; [d] very broad lines, ($\Delta v \geq$ 15 km s^{-1}), due to the blending of several excited ethyl cyanide transitions and/or to the blending with an unknown species.
The dashes indicates that the value is the same as the one in the previous line.

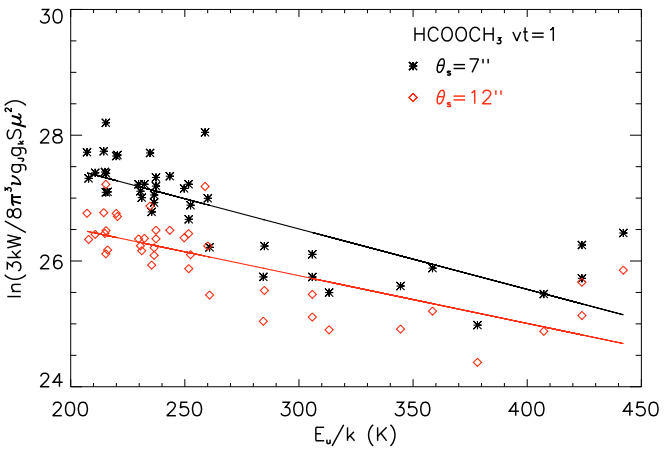

Fig. 2. Rotational diagram of the torsionally excited state of methyl formate for different source sizes. For a source size of 7″ (black stars), we found a rotational temperature of T_{rot} = 104 ± 14 K and a column density of $N = 9.4^{+4.0}_{-2.8} \times 10^{16}$ cm^{-2}; for a source size of 12″ (red diamonds), we found T_{rot} = 131 ± 20 K and $N = 3.4^{+1.5}_{-1.1} \times 10^{16}$ cm^{-2}.

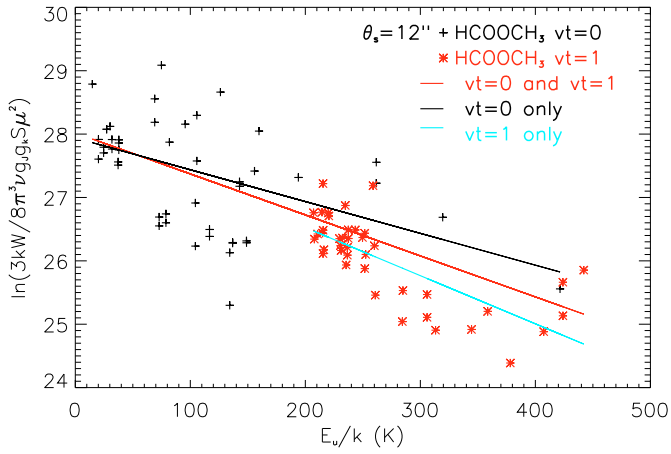

Fig. 3. Rotational diagram of methyl formate in the ground state (black crosses) and methyl formate in both the ground and excited states (red stars). The source size is 12″. The rotational temperature and column density for methyl formate in the ground state are T_{rot} = 199 ± 28 K and $N = 9.6^{+0.9}_{-0.9} \times 10^{16}$ cm^{-2} and T_{rot} = 154 ± 8 K and $N = 5.6^{+4.0}_{-3.7} \times 10^{16}$ cm^{-2} when the ground and the first torsionally excited state are combined. For comparison, the rotational diagram for the excited state only is plotted (blue curve).

This paper presents the molecular theory used for the spectral analysis of new measurements of excited ethyl cyanide in the 85–400 GHz range for $J \leq 50$ and $K_a \leq 15$. However, the complete analysis has not yet been published and the prediction for the line frequencies and intensities was obtained from J. Pearson (private communication).

Most lines belonging to the excited states $\upsilon_t = 1$ and $\upsilon_b = 1$ are blended with other strong lines, identified or not (Table 3). However, few lines allow the column density of vibrationally excited ethyl cyanide to be constrained (Table 3). We estimated the upper limit to the abundance of excited CH_3CH_2CN by comparing the emission spectrum of excited ethyl cyanide simulated

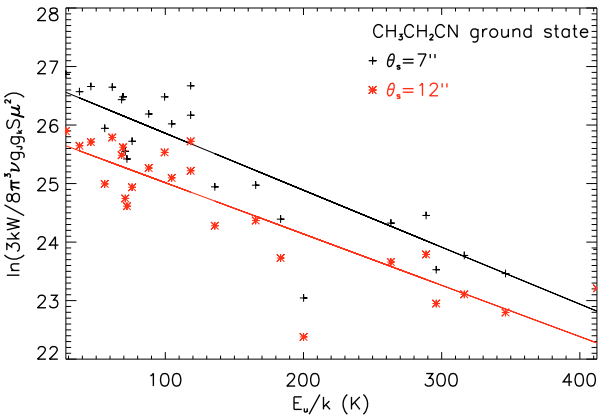

Fig. 4. Rotational diagram of the ethyl cyanide in the ground state for different source sizes. For a source size of 7″ (black crosses) we find a rotational temperature of $T_{\rm rot}$ = 103 ± 9 K and a column density of $N = 3.7^{+0.6}_{-0.5} \times 10^{15}$ cm^{-2}; for a source size of 12″ (red stars) we find $T_{\rm rot}$ = 114 ± 11 K and $N = 1.3 \times 10^{16} \times 10^{15}$ cm^{-2}.

and the LTE model with the observed spectra, for different temperatures and column densities (Fig. 5). Adopting the same temperature as the ground state (100 K) and a higher temperature of 200 K, we found that the column density of vibrationally excited ethyl cyanide is 10^{16} cm^{-2} and 5×10^{15} cm^{-2}, respectively.

6. Methyl carbamate and glycine

The initial aim of the observations was to search for methyl carbamate (NH_2COOCH_3), an isomer of glycine (NH_2CH_2COOH). Methyl carbamate has a strong dipole moment and is energetically more stable than glycine, two reasons that make it a good candidate for interstellar detection. The rotational spectrum of methyl carbamate in the A torsional substate was studied in the 8–240 GHz frequency range (Bakri et al. 2002; Ilyushin et al. 2006). This study was extended by Groner et al. (2007), who measured transitions of both A and E torsional substates up to 371 GHz. Our first analysis of the observations from 2003 was performed with a prediction of lines frequencies and intensities produced for the A-transitions from the work of Bakri et al. (2002). We then completed a revised analysis of our data from 2003 and 2006 with the predictions given by Groner et al. (2007).

Several tens of lines from methyl carbamate were searched in spectral regions chosen carefully to avoid or limit confusion with spectral lines from other molecules. However, we did not detect methyl carbamate in our data. Furthermore, most of the lines were fully blended and only a few lines allowed us to constrain an upper limit to the abundance of methyl carbamate in W51 e2. By comparing the simulated emission spectrum of methyl carbamate at different temperatures and source sizes with the observed spectrum (Fig. 6), we constrained the upper limit of methyl carbamate in this source. For a small emission region (7″) and warm gas (200 K), we found that $N \leq 5 \times 10^{14}$ cm^{-2}. This upper limit decreases as the rotational temperature and/or the size of the emission source decreases. We measured $N \leq 2 \times 10^{14}$ cm^{-2} for $T_{\rm rot}$ = 100 K, and $\theta_{\rm s}$ = 12″, and $N \leq 8 \times 10^{13}$ cm^{-2} for $T_{\rm rot}$ = 50 K and $\theta_{\rm s}$ = 30″.

Numerous transitions from both conformers of glycine are within our observed spectral ranges. Glycine is not detected in the spectra. Almost all lines are blended and only a few can be used to estimate roughly the upper limit of glycine in W51 e2.

Table 4. Temperature and column density of the detected molecules.

Molecules		Source size	
		7″	12″
$HCOOCH_3$	T (K)	176 ± 24	199 ± 28
$\upsilon_t = 0$	N (cm^{-2})	$17.0^{+1.8}_{-1.6} \times 10^{16}$	$9.6^{+0.9}_{-0.9} \times 10^{16}$
$HCOOCH_3$	T (K)	104 ± 14	131 ± 20
$\upsilon_t = 1$	N (cm^{-2})	$9.4^{+4.0}_{-2.8} \times 10^{16}$	$3.4^{+1.5}_{-1.1} \times 10^{16}$
$HCOOCH_3$	T (K)	144 ± 7	154 ± 8
$\upsilon_t = 0 + \upsilon_t = 1$	N (cm^{-2})	$11.4^{+0.9}_{-0.8} \times 10^{16}$	$5.6^{+4.0}_{-3.7} \times 10^{16}$
CH_3CH_2CN	T (K)	103 ± 9	114 ± 11
	N (cm^{-2})	$3.7^{+0.6}_{-0.5} \times 10^{15}$	$1.7^{+0.3}_{-0.2} \times 10^{15}$

This upper limit varies by an order of magnitude depending on the source size and rotational temperature. Assuming a rotational temperature of 100 K, the upper limit to the column density of glycine is 3×10^{14} cm^2 for a 7″ source size, and 6×10^{13} cm^2 for a 30″ source size.

7. Discussion

We have found that the rotational temperatures derived from our rotational diagram analysis differ from the kinetic temperature, $T_{\rm kin}$ = 153(21) K, derived by Remijan et al. (2004). The rotational temperature of ethyl cyanide, of between 103 K and 114 K, is lower than $T_{\rm kin}$, independent of the adopted source size. It is higher than $T_{\rm kin}$ if we consider methyl formate in its ground state (176–199 K), lower if we consider only the excited state (104–131 K), and of the same order if we consider simultaneously the ground state and the first excited state of methyl formate (144–154 K). This appears to indicates that the LTE hypothesis is probably not fully valid. However, despite this possible departure from LTE, the rotational diagram method, which assumes implicitly that LTE has been reached and that all temperatures are equivalent (i.e. $T_{\rm exc} = T_{\rm kin} = T_{\rm rot} = T_{\rm vib}$), is the only method that can be used to estimate the excitation temperature since a statistical analysis is ruled out by the absence of known collision rates for the studied molecules.

The relevance of the LTE assumption within each rotational level may also be evaluated by comparing the cloud density to the critical density of each vibrational state. Collisional rates are not known for molecules as complex as methyl formate or ethyl cyanide. However, it is possible to estimate roughly the critical density for these molecules by adopting the value of methanol interacting with H_2, of the order of a few 10^{-11} cm^3 s^{-1} (Pottage et al. 2004), and by assuming that it is the same for the ground and vibrational excited states. The Einstein coefficients of the rotational transitions are in the range 10^{-5}–10^{-6} s^{-1}. The critical density is therefore approximately 10^5–10^6 cm^{-3}, i.e. comparable to the hydrogen density in W51 e2, which is estimated to be $n_{\rm H} = 5(2) \times 10^5$ cm^{-3} (Remijan et al. 2004). There is thus a competition between collisional and radiative excitation and it is clear that the levels are probably not all thermalized.

The excitation mechanism populating the observed excited state of methyl formate and ethyl cyanide may be inferred in a similar way. The Einstein coefficients for ro-vibrational transitions from the excited states to the ground state are of the order of a few 10^{-1} s^{-1}, far higher than for rotational transitions within the excited state (10^{-5}–10^{-6} s^{-1}). Adopting the same value for the collisional rate as before (a few 10^{-11} cm^3 s^{-1}), the density needed to thermalize the levels in the excited state by collisions must therefore be higher than the critical density, which is of the order of 10^{10} cm^{-3}. The dust in W51 e2 has a temperature

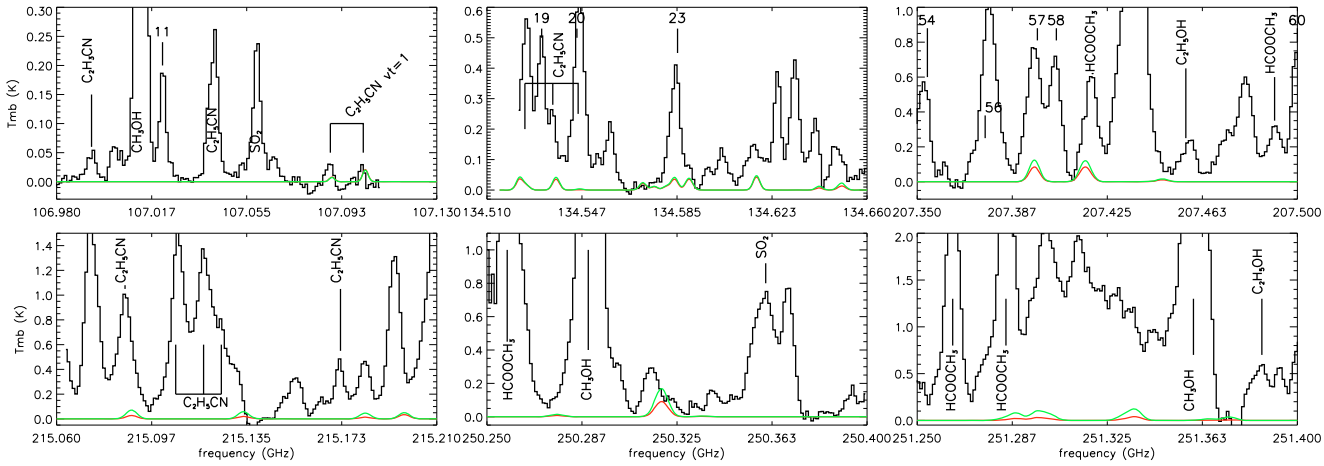

Fig. 5. Detected lines from the first two excited states $\upsilon_t = 1$ and $\upsilon_b = 1$ of ethyl cyanide CH_3CH_2CN. The observations (histogram like curve) were compared with LTE emission models of CH_3CH_2CN $\upsilon_t = 1$ and $\upsilon_b = 1$ with $\theta_s = 7''$, $T = 100$ K and $N = 10^{16}$ cm^{-2} (red curve) and $T = 200$ K and $N = 5 \times 10^{15}$ cm^{-2} (green curve). The numbered lines are excited methyl formate lines (see Table 2). See Table 3 for the identification of the excited CH_3CH_2CN lines.

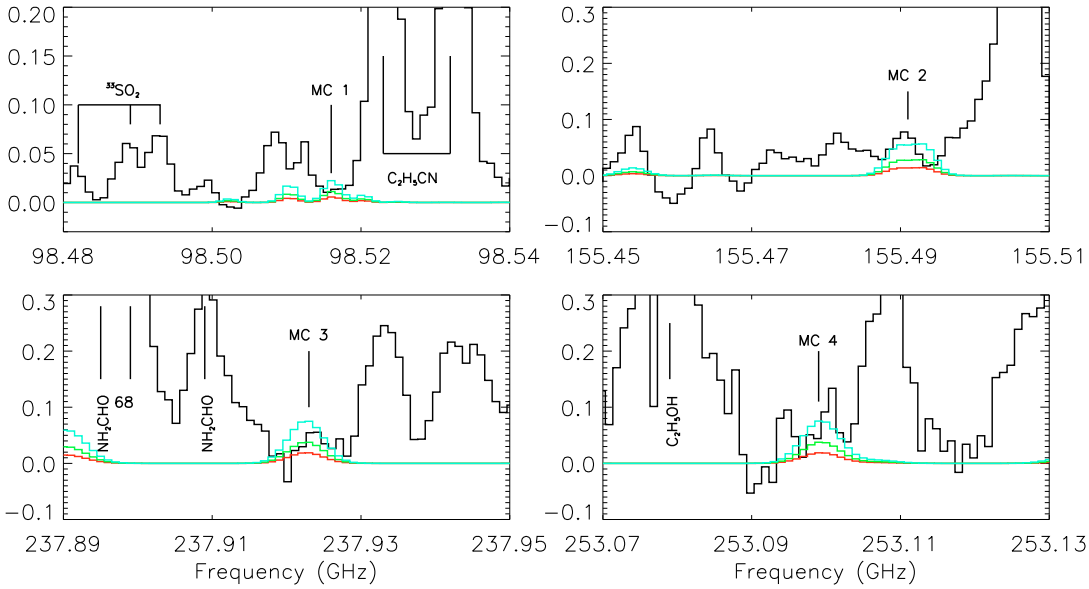

Fig. 6. Observed spectrum of W51 e2 (histogram like curve) compared with the LTE emission spectrum of methyl carbamate at different densities, for a 12″ source and rotational temperature of 100 K: red curve: $N = 10^{14}$ cm^{-2}, green curve: $N = 2 \times 10^{14}$ cm^{-2}, blue curve: $N = 4 \times 10^{14}$ cm^{-2}. The methyl carbamate lines are (from Groner et al. 2007): MC1: $14_{2,13}-13_{1,12}$ (E) at 98515.38 GHz and $15_{1,15}-14_{0,14}$ E and A at 98516.99 GHz; MC2: $23_{1,22}-22_{2,21}$ at 155489.10 and 155492.68 GHz for the E and A symmetry, respectively and $23_{2,22}-22_{1,21}$ at 155490.07 and 155493.65 GHz for the E and A symmetry, respectively; MC3 : $14_{10,5}-13_{9,4}$ (A) and $14_{10,4} - 13_{9,5}$ (A) (blended) at 237922.60 GHz; MC4: $16_{10,7}-15_{9,6}$ (A) and $16_{10,6}-15_{9,7}$ (A) at 253099.30 and 253099.37 GHz, respectively.

of about 140 K (Sollins et al. 2004) and emits efficiently at the wavelength of the excited states of both molecules. It is thus most probable that the excited states of methyl formate and ethyl cyanide are populated by radiative processes rather than collisions.

We have found that the rotational temperature of the gas decreases as the source size becomes smaller. This is surprising since it is expected that the deepest regions of hot cores are also the warmest. The observed transitions are optically thin for the adopted source sizes of 12″ and 7″. BIMA observations of methyl formate in W51 e2 (Remijan et al. 2002) showed that the emission region is smaller for high energy transitions than for low energy transitions. The size of the emission region was around 12″ for the $7_{2,5}$–$6_{2,4}$ transition at 90 146 MHz, corresponding to an energy of 10 cm^{-1} (15 K), and around 7″ for the $18_{5,13}$–$17_{5,12}$ transition at 228 629 MHz, corresponding to an energy of 75 cm^{-1} (108 K). More interferometric observations are required to locate precisely the emission region of methyl formate and ethyl cyanide in the ground and excited state and understand their temperature distribution.

The presence of methyl formate in torsional excited state in hot cores such as W51 e2 and Orion KL (Kobayashi et al. 2007) is unsurprising. Methyl formate is abundant and its torsional mode has low energy (188 K). Similarly, it is unsurprising that ethyl cyanide is more difficult to detect: it is less abundant and its excited states are at slightly higher energy, around 300 K. However, it is clear that observations of higher signal-to-noise ratio, spectral, and angular resolution, such as forthcoming

observations from Herschel and ALMA, will reveal far more lines from the excited states of these molecules but also of abundant large molecules possessing low-frequency vibrational states. For example, dimethyl ether, CH_3OCH_3, has two torsional modes at about 203 and 242 cm^{-1} and transitions from these modes should be present in the spectra of hot cores. More generally, a large number of unidentified lines reported in the spectra of hot molecular clouds could be due to transitions from abundant molecules in excited states.

Acknowledgements. The authors would like to thank Alexandre Faure for fruitful discussions, Jean Demaison and Isabelle Kleiner for invaluable help in the methyl formate study and John Pearson for providing us with the excited ethyl cyanide spectrum. We acknowledge all the Pico Veleta IRAM staff for their help during the observations. We thank the referee for his/her constructive comments. This work was supported by the Programme National "Physico Chimie du Milieu Interstellaire" and by the European Research Training Network "Molecular Universe" (MRTN-CT-2004-512302). M.C. thanks the CNRS (project CERC3) and Junta de Andalucia (project P07-FQM-03014) for financial support.

References

Bakri, B., Demaison, J., Kleiner, I., et al. 2002, J. Mol. Spectrosc., 215, 312
Carvajal, M., Willaert, F., Demaison, J., & Kleiner, I. 2007, J. Mol. Spectrosc., 246, 158
Demaison, J., Boucher, D., & Dubrulle, A. 1984, J. Mol. Spectrosc., 102, 260
Fuchs, G. W., Fuchs, U., Giesen, T. F., & Wyrowski, F. 2005, A&A, 444, 521
Fukuyama, Y., Omori, K., Odashima, H., Takagi, K., & Tsunekawa, S. 1999, J. Mol. Spectroscopy, 193, 72
Gordy, W., & Cook, R. L. 1984, Microwave Molecular Spectra (New York: John Wiley & Sons)
Groner, P., Winnewisser, M., Medvedev, I. R., et al. 2007, ApJS, 169, 28
Hollis, J. M., Lovas, F. J., Remijan, A. J., et al. 2006, ApJ, 643, L25
Hougen, J. T., Kleiner, I., & Godefroid, M. 1994, J. Mol. Spectroscopy, 163, 559
Ikeda, M., Ohishi, M., Nummelin, A., et al. 2001, ApJ, 560, 792
Ilyushin, V., Alekseev, E., Demaison, J., & Kleiner, I. 2006, J. Mol. Spectroscopy, 240, 127
Ilyushin, V., Kleiner, I., & Lovas, F. J. 2008, J. Physical and Chemical Reference Data, 37, 97
Kleiner, I., Lovas, F. J., & Godefroid, M. 1996, J. Physical and Chemical Reference Data, 25, 1113
Kobayashi, K., Ogata, K., Tsunekawa, S., & Takano, S. 2007, ApJ, 657, L17
Liu, S.-Y., Mehringer, D. M., & Snyder, L. E. 2001, ApJ, 552, 654
Mehringer, D. M., Pearson, J. C., Keene, J., & Phillips, T. G. 2004, ApJ, 608, 306
Nummelin, A., Bergman, P., Hjalmarson, A., et al. 1998, ApJS, 117, 427
Oesterling, L. C., Albert, S., De Lucia, F. C., Sastry, K. V. L. N., & Herbst, E. 1999, ApJ, 521, 255
Ogata, K., Odashima, H., Takagi, K., & Tsunekawa, S. 2004, J. Mol. Spectroscopy, 225, 14
Plummer, G. M., Herbst, E., De Lucia, F., & Blake, G. A. 1984, ApJS, 55, 633
Plummer, G. M., Herbst, E., De Lucia, F. C., & Blake, G. A. 1986, ApJS, 60, 949
Pottage, J. T., Flower, D. R., & Davis, S. L. 2004, MNRAS, 352, 39
Remijan, A., Snyder, L. E., Liu, S.-Y., Mehringer, D., & Kuan, Y.-J. 2002, ApJ, 576, 264
Remijan, A., Sutton, E. C., Snyder, L. E., et al. 2004, ApJ, 606, 917
Snyder, L. E., Lovas, F. J., Hollis, J. M., et al. 2005, ApJ, 619, 914
Sollins, P. K., Zhang, Q., & Ho, P. T. P. 2004, ApJ, 606, 943
Turner, B. E. 1991, ApJS, 76, 617
Zhang, Q., Ho, P. T. P., & Ohashi, N. 1998, ApJ, 494, 636